Supplementary information

A detailed description of the original model, including derivation of all equations, model calibration, lists of used parameters, and sensitivity analyses can be found in Wing & Halevy (2014) and the supporting information therein. Here we present all modifications to the original model as well as their implications.

Stoichiometry of redox reactions

When not stated differently, we always used the simplest possible case to find absolute limits on maximum achievable S isotope fractionation. This means we assumed that only one electron carrier transfers electrons to Apr, and only one electron carrier transfers the 6 electrons to DsrAB, partly through the DsrC cycle (Table S2). When special cases were explored, e.g., several proposed electron confurcation schemes for APS reduction, and a stepwise reduction of SO_3^{2-} with 2 different electron carriers, it is explicitly mentioned in the main text.

Linking S isotope fractionation, sulfate availability in the cell's environment, and csSRR to enzyme kinetics and to reaction thermodynamics.

The net rate (J) of a reversible enzymatic reaction can be expressed as (Flamholz et al., 2013):

$$J = V_{max} \times \frac{\prod_j \left(\frac{[r_j]}{K_{Mj}}\right)^{n_j}}{1 + \prod_j \left(\frac{[r_j]}{K_{Mj}}\right)^{n_j} + \prod_i \left(\frac{[p_i]}{K_{Mi}}\right)^{m_i}} \times \left(1 - e^{\frac{\Delta G_r}{RT}}\right), \qquad (8)$$

where V_{max} is the maximum metabolic rate capacity, $[r_j]$ is the concentration of the reactant *j*, K_{Mj} is the half-saturation constant of the reactant *j* at the enzyme, $[p_i]$ is the concentration of the product *i*, and K_{Mi} is the half-saturation constant of the product *i* at the enzyme. n_j and m_i are the stoichiometric coefficients of the reactant *j* and the product *i*, respectively. Combining equations 6 and 7 from the main text with equation 8 above for each step of the linear metabolic reaction network, solving for *f* of each step, and substituting in equations 2-5 from the main text, ultimately links the overall isotope fractionation to the reaction rate, to intracellular and extracellular metabolite concentrations, to enzyme kinetic parameters, and to the Gibbs free energies of the reactions. Rate-fractionation relationships and their dependence on sulfate concentrations and temperature, as well as a set of experimentally accessible biochemical information are available for DSR, which has allowed calibration of the model and the quantitative prediction of S isotope fractionation as a function of physiological, enzymatic, and environmental conditions (Wing & Halevy, 2014).

Reversibility of enzymatic reactions during DSR.

The observation of large fractionation at low respiration rates requires reversibility of all steps during DSR. Sulfate uptake into the cell, sulfate activation to APS, and APS reduction to SO_3^{2-} are fully reversible steps (Trüper & Fischer, 1982; Cypionka, 1995; Frigaard & Dahl, 2009). Whether or not the full enzyme-catalyzed SO_3^{2-} reduction to H_2S can also proceed in the reverse direction during DSR is unclear. It has been suggested that at least the first reduction step, i.e., the transfer of the first 2 electrons from an

unknown physiological electron donor to SO_3^{2-} is reversible (Brunner et al., 2012). Whether or not the DsrC cycle is reversible in sulfate-reducing organisms is debated, even though the observed transfer of a ^{35}S spike from extracellular product sulfide to extracellular substrate sulfate in growing cultures of sulfate reducing microbes suggests at least some degree of reversibility (Trudinger & Chambers, 1973; Holler et al., 2011). Importantly, even if future work shows that this last H_2S-forming step is irreversible, our model predictions and the results of this study remain valid, as large equilibrium fractionation exists between SO_3^{2-} and S^0 (60‰ at 25°C; Otake et al. (2008)), which is a probable intermediate in the reduction of SO_3^{2-} to H_2S. Hence, strictly speaking, large fractionation at low respiration rates as observed in culture experiments and in natural environments requires nearly full reversibility of all reactions upstream of the H_2S-forming step.

$R_{r/o}$, K_M values, and electron carrier identity limit achievable S isotope fractionation.

Large fractionation (>55‰) is only possible when each step during DSR is close to the thermodynamic limit (Fig. 1) and each reversibility term (*f*) in equations 2 to 5 approaches unity. In order to identify the most sensitive parameters controlling this reversibility, we combined equations 6, 7, and 8 and solved for *f*. For the example of APS reduction to SO_3^{2-} and adenosine monophosphate (AMP), the metabolic reaction is:

$$\mathrm{APS} + \frac{2}{n}\mathrm{EC_{red}} \rightleftharpoons \mathrm{SO_3^{2-}} + \mathrm{AMP} + \frac{2}{n}\mathrm{EC_{ox}}, \quad (9)$$

where *n* is the number of electrons carried by the respective electron carrier involved in APS reduction. The reversibility of this reaction ($f_{SO32-,APS}$) is a direct function of the Gibbs free energy (equation 6), which for the APS reduction step is:

$$\Delta G_r = \Delta G'^{\circ} + RTln\left(\frac{[SO_3^{2-}][AMP][EC_{ox}]^{\frac{2}{n}}}{[APS][EC_{red}]^{\frac{2}{n}}}\right). \quad (10)$$

In order for $f_{SO32-,APS}$ to approach 1, ΔG_r must approach 0 (equation 6). The standard-state Gibbs free energy, $\Delta G'^{\circ}$, can be calculated from the stoichiometry of the metabolic reaction and the redox potentials of the half reactions (APS → AMP + HSO_3^-, and EC_{ox} → EC_{red}) at standard-state conditions, and approximately varies from -60 kJ mol^{-1} for APS reduction with ferredoxin to 21 kJ mol^{-1} for APS reduction with rubrerythrin, respectively (Table S3). Intracellular AMP concentrations have been measured in a model sulfate reducer (Yagi & Ogata, 1996) and are here maintained constant at 0.3 mM. For illustration, we assume that menaquinone is the physiological electron donor to sulfite reductase. In this situation, sulfite concentrations are controlled by cell external H_2S concentrations and are therefore constant for specified experimental conditions (Wing & Halevy, 2014). APS concentrations at steady state can then be calculated by modifying equation 8 and solving for [APS]:

$$[APS] = \frac{\frac{J}{v_{max}} K_{M(APS)} K_{M(EC_{red})}^{\frac{2}{n}}}{[EC_{red}]^{\frac{2}{n}}\left(1 - \frac{J}{v_{max}}\right)} + \cdots$$

$$\ldots + \frac{\frac{J}{v_{max}} K_{M(APS)} K_{M(EC_{red})}^{\frac{2}{n}} [SO_3^{2-}][AMP][EC_{ox}]^{\frac{2}{n}}}{[EC_{red}]^{\frac{2}{n}}\left(1 - \frac{J}{v_{max}}\right) K_{M(SO_3^{2-})} K_{M(AMP)} K_{M(EC_{ox})}^{\frac{2}{n}}} + \cdots$$

$$\ldots + \frac{[SO_3^{2-}][AMP][EC_{ox}]^{\frac{2}{n}} e^{\frac{\Delta G'^{\circ}}{RT}}}{[EC_{red}]^{\frac{2}{n}}\left(1-\frac{J}{v_{max}}\right)}. \quad (11)$$

In the expression in equation 10, ΔG_r decreases with increasing [APS]. Equation 11 reveals that three model parameters control [APS] and, therefore, ΔG_r and the reversibility of the reaction at a specific respiration rate: *i)* the standard-state Gibbs free energy of the reaction, *ΔG'°*, which appears in the third term in the right-hand side of equation 11, *ii)* the ratio of reduced to oxidized electron carrier concentrations ($R_{r/o}$ = [EC_{red}] / [EC_{ox}]), which appears in all three terms in the right-hand side of the equation, and *iii)* enzyme kinetic parameters, which appear in the first two terms. As outlined above, *ΔG'°* depends directly on the identity and reduction potential of the electron carrier involved (Table S3). Little is known about the value of $R_{r/o}$ in sulfate reducers. We therefore varied $R_{r/o}$ over a wide range of values and explored the dependence of the maximum achievable S isotope fractionation on this parameter (Fig. 4). Enzyme kinetic parameters, and specifically the half saturation concentrations, are relatively well constrained from independent biochemical experiments (Dataset S1). Nevertheless, we here allowed K_M values to vary within a larger range than suggested from experimental data in order to explore the dependence of the reversibility of the reaction, and the maximum achievable S isotope fractionation, on these parameters.

Sensitivity of maximum achievable S isotope fractionation to K_M values.

Besides the standard-state Gibbs free energies of each reaction step and $R_{r/o}$, enzyme kinetic parameters, specifically the half-saturation constants, potentially control the

reversibility of the steps and hence fractionation at low respiration rates. With some exceptions K_M values are relatively well constrained from independent biochemical analyses in several sulfate reducing bacteria and archaea, and most of those values lie between 10 μM and 400 μM (see Dataset S1) (Bramlett & Peck, 1975; Lampreia et al., 1994; Wolfe et al., 1994; Yagi & Ogata, 1996; Fritz et al., 2002). All default values used in this study are given in Table S5 and are indicated with horizontal grey lines in Fig. S1. A relatively narrow range of K_M values is also observed in many other catalytic reactions. Bar-Even et al. (2011) analyzed reported enzyme kinetic parameters of thousands of enzymes from prokaryotic and eukaryotic organisms and found that 60% of all K_M values range between 10 μM and 1000 μM, with a median value of 130 μM, and that over 99% of all analyzed enzymes have K_M values > 0.1 μM. We therefore explored the sensitivity of the maximum achievable S isotope fractionation to each of the substrate K_M values in the Apr- and Dsr-catalyzed reactions within the range of 0.1 μM to 100 mM. For a given electron carrier, reversibility decreases exponentially with increasing K_M values for the substrates in the given metabolic reactions (APS in the Apr-catalyzed reaction and SO_3^{2-} in the Dsr-catalyzed reaction; Fig. S1A, B). On the other hand, the reversibility increases exponentially with increasing K_M values for the products in the given metabolic reactions (SO_3^{2-} and AMP in the Apr-catalyzed reaction and H_2S in the Dsr-catalyzed reaction; Fig. S1E, F, G). The reversibility of APS reduction is not sensitive to the K_M value of the electron carrier under the assumption that the reduced and oxidized forms of the electron carrier have identical K_M values (Fig. S1C). The reversibility of SO_3^{2-} reduction is sensitive to the K_M value of the electron carrier only if K_M values are very large (> 1 mM).

Lowering the K_M value to below this threshold does not affect the reversibility of the reaction, and thus the maximum achievable S isotope fractionation (Fig. S1D).

In order to isolate the influence of electron carrier identity on the absolute limit on maximum achievable S isotope fractionations (Fig. 3B), we chose a set of extreme K_M values that maximized the reversibility effects discussed above (Table S5; Dataset S1). Whenever there was a reported range of K_M values we chose the value that yielded the largest possible reversibility (fractionation) at the lowest possible $\Delta G'°$. No data exists on $K_M(H_2S)$ in the Dsr-catalyzed reaction, and we therefore use the upper limit of 100 mM (Bar-Even et al., 2011) as our extreme value (Fig. S1F; Table S5). Moreover, some studies suggest that K_M(APS) in the Apr-catalyzed reaction might be unusually small (<20 μM, (Fritz et al., 2002) or ≈1 μM, (Yagi & Ogata, 1996). We let this K_M value to vary over an even larger range than suggested based on Bar-Even et al. (2011), and set the most extreme value to 1 nM (Fig. S1A; Table S5). Importantly, even at these extremes, it is not possible to achieve large fractionation at low csSRR for some electron carriers (Fig. 3B). The reason for this is that even at the most extreme K_M values (Table S5; Fig. S1), the energetics of APS and SO_3^{2-} reduction with some electron donors are too favorable to ever achieve near-reversibility ($f \rightarrow 1$) and large (near-equilibrium) isotope fractionation. As in the case of varying $R_{r/o}$, the largest fractionation achievable depends on the $\Delta G'°$ of the reactions in the DSR pathway, and hence, on the standard redox potential and the identity of the physiological electron carriers involved in APS and SO_3^{2-} reduction. In summary, $R_{r/o}$ and K_M values affect the shape of the transition from the smallest possible to the largest possible fractionation, but eventually it is the identity of

144 the electron carrier that controls the magnitude of the minimum and maximum
145 fractionation.

Table S1. Two criteria that need to be fulfilled by any proposed energy metabolism scheme for dissimilatory sulfate reduction.

Criterion	Methodological approach
1. Large S isotope fractionation at low csSRR	a) Vary $R_{r/o}$ to extremes b) Vary K_M values to extremes c) Find limits on $\Delta G'^{\circ}$
2. Reasonable intracellular metabolite concentrations	Find limits on $R_{r/o}$ for electron carriers that fulfilled criterion 1.

Table S2. Metabolic redox reactions during dissimilatory sulfate reduction.

Description	Reaction
APS reduction	
APS reduction with one electron carrier (EC) that carries *n* electrons	$\mathrm{APS} + \frac{2}{n}\mathrm{EC_{red}} \rightleftharpoons \mathrm{SO_3^{2-}} + \mathrm{AMP} + \frac{2}{n}\mathrm{EC_{ox}}$
Example of electron confurcation scheme for APS reduction	$\mathrm{APS} + 0.5\mathrm{MKH_2} + \mathrm{FH} \rightleftharpoons \mathrm{SO_3^{2-}} + \mathrm{AMP} + 0.5\mathrm{MK} + \mathrm{F}$
SO_3^{2-} reduction	
SO_3^{2-} reduction with one electron carrier (EC) that carries *n* electrons	$\mathrm{SO_3^{2-}} + \frac{6}{n}\mathrm{EC_{red}} \rightleftharpoons \mathrm{H_2S} + \frac{6}{n}\mathrm{EC_{ox}}$
SO_3^{2-} reduction with an EC transferring 2 and MKH_2 transferring 4 electrons	$\mathrm{SO_3^{2-}} + \frac{2}{n}\mathrm{EC_{red}} + 2\mathrm{MKH_2} \rightleftharpoons \mathrm{H_2S} + \frac{2}{n}\mathrm{EC_{ox}} + 2\mathrm{MK}$
SO_3^{2-} reduction to DsrC-bound S° trisulfide with an EC transferring 2 and $DsrC_{red}$ transferring another 2 electrons	$\mathrm{SO_3^{2-}} + \frac{2}{n}\mathrm{EC_{red}} + \mathrm{DsrC_{red}} \rightleftharpoons \mathrm{S^\circ\ DsrC_{ox}} + \frac{2}{n}\mathrm{EC_{ox}}$
DsrC-bound S° trisulfide reduction to H_2S and recycled $DsrC_{red}$	$\mathrm{S^\circ\ DsrC_{ox}} + 2\mathrm{MKH_2} \rightleftharpoons \mathrm{H_2S} + \mathrm{DsrC_{red}} + 2\mathrm{MK}$

n is the number of electrons carried by the respective electron carrier (EC). MKH_2 = menaquinol; MK = menaquinone; F = flavodoxin (quinone); FH = flavodoxin (semiquinone); $\mathrm{S^\circ\ DsrC_{ox}}$ = DsrC-bound S° trisulfide. See main text for more information.

Table S3. Reduction potentials and standard-state Gibbs free energies used in the model.

Redox compound	E'° [mV]*	$\Delta G'°$ of APS reduction [kJ mol^{-1}]	$\Delta G'°$ of SO_3^{2-} reduction [kJ mol^{-1}]**	$\Delta G'°$ of SO_3^{2-} reduction [kJ mol^{-1}]***
Ferredoxin ox/red	-398	-60.4	-174.5	-41.0
Flavodoxin FH/FH_2	-371	-55.2	-158.8	-35.8
Cytochrome c3 ox/red	-290	-39.6	-111.9	-20.2
Flavodoxin F/FH	-115	-5.8	-10.6	13.6
MK/MKH_2	-74	4.4	20.1	20.1
Rubredoxin ox/red	-57	5.4	23.0	24.8
Rubrerythrin ox/red	23	20.8	69.3	40.2

* Values taken from Thauer et al. (1977).

** The redox compound is the only electron donor.

*** The redox compound transfers the first 2 electrons and the remaining 4 are originating from menaquinol oxidation.

Table S4. Reduced to oxidized electron carrier concentrations at low respiration rates determined in this study.*

Electron carrier (EC)	$[EC_{red}]/[EC_{ox}]$
Menaquinone	20
Flavodoxin	0.7
Rubredoxin	5
Rubrerythrin	100

* The values are taken from the diagonal plots in Fig. 5, i.e. assuming that a single electron carrier transfers electrons to both Apr and Dsr.

167 **Table S5. Reasonable (default) and extreme K_M values used in the model.**

Reaction		default K_M [mM]	extreme K_M* [mM]
$\mathrm{APS} + \frac{2}{n}\mathrm{EC_{red}} \rightleftharpoons \mathrm{SO_3^{2-}} + \mathrm{AMP} + \frac{2}{n}\mathrm{EC_{ox}}$			
	APS	0.02	0.000001
	EC	0.1	0.2
	SO_3^{2-}	0.4	1.3
	AMP	0.3	0.4
$\mathrm{SO_3^{2-}} + \frac{6}{n}\mathrm{EC_{red}} \rightleftharpoons \mathrm{H_2S} + \frac{6}{n}\mathrm{EC_{ox}}$			
	SO_3^{2-}	0.05	0.012
	EC	0.02	0.02
	H_2S	0.01	100

168 * Used only in Fig. 3B.

169

References

Bar-Even A, Noor E, Savir Y, Liebermeister W, Davidi D, Tawfik DS*, et al.* (2011). The moderately efficient enzyme: Evolutionary and physicochemical trends shaping enzyme parameters. *Biochemistry.* 50**:** 4402-4410.

Bramlett RN & Peck HD. (1975). Some physical and kinetic properties of adenylyl sulfate reductase from *Desulfovibrio vulgaris*. *J. Biol. Chem.* 250**:** 2979-2986.

Brunner B, Einsiedl F, Arnold GL, Muller I, Templer S, Bernasconi SM. (2012). The reversibility of dissimilatory sulphate reduction and the cell-internal multi-step reduction of sulphite to sulphide: insights from the oxygen isotope composition of sulphate. *Isot. Environ. Health Stud.* 48**:** 33-54.

Cypionka H. (1995). Solute transport and cell energetics. *In:* Barton LL (ed.) *Sulphate-reducing bacteria.* New York: Plenum Press.

Flamholz A, Noor E, Bar-Even A, Liebermeister W, Milo R. (2013). Glycolytic strategy as a tradeoff between energy yield and protein cost. *Proceedings of the National Academy of Sciences of the United States of America.* 110**:** 10039-10044.

Frigaard NU & Dahl C. (2009). Sulfur metabolism in phototrophic sulfur bacteria. *In:* Poole RK (ed.) *Advances in Microbial Physiology.* London: Academic Press Ltd-Elsevier Science Ltd.

Fritz G, Buchert T, Kroneck PMH. (2002). The function of the 4Fe-4S clusters and FAD in bacterial and archaeal adenylylsulfate reductases - Evidence for flavin-catalyzed reduction of adenosine 5 '-phosphosulfate. *J. Biol. Chem.* 277**:** 26066-26073.

191 Holler T, Wegener G, Niemann H, Deusner C, Ferdelman TG, Boetius A*, et al.* (2011).
192 Carbon and sulfur back flux during anaerobic microbial oxidation of methane and
193 coupled sulfate reduction. *Proceedings of the National Academy of Sciences.* 108**:**
194 1484-1490.
195 Lampreia J, Pereira AS, Moura JJG. (1994). Adenylylsulfate reductases from sulfate-
196 reducing bacteria. *Methods Enzymol.* 243**:** 241-260.
197 Otake T, Lasaga AC, Ohmoto H. (2008). Ab initio calculations for equilibrium
198 fractionations in multiple sulfur isotope systems. *Chem. Geol.* 249**:** 357-376.
199 Thauer RK, Jungermann K, Decker K. (1977). Energy conservation in chemotrophic
200 anaerobic bacteria. *Bacteriological Reviews.* 41**:** 100-180.
201 Trudinger PA & Chambers LA. (1973). Reversibility of bacterial sulfate reduction and its
202 relevance to isotope fractionation. *Geochimica Et Cosmochimica Acta.* 37**:** 1775-
203 1778.
204 Trüper HG & Fischer U. (1982). Anaerobic oxidation of sulfur compounds as electron
205 donors for bacterial photosynthesis. *Philos. Trans. R. Soc. Lond. Ser. B-Biol. Sci.*
206 298**:** 529-542.
207 Wing BA & Halevy I. (2014). Intracellular metabolite levels shape sulfur isotope
208 fractionation during microbial sulfate respiration. *Proceedings of the National*
209 *Academy of Sciences of the United States of America.* 111**:** 18116-18125.
210 Wolfe BM, Lui SM, Cowan JA. (1994). Desulfoviridin, a multimeric-dissimilatory sulfite
211 reductase from *Desulfovibrio vulgaris* (Hildenborough) - Purification,
212 characterization, kinetics and EPR studies. *Eur. J. Biochem.* 223**:** 79-89.

213 Yagi T & Ogata M. (1996). Catalytic properties of adenylylsulfate reductase from
214 Desulfovibrio vulgaris Miyazaki. *Biochimie.* 78**:** 838-846.

215

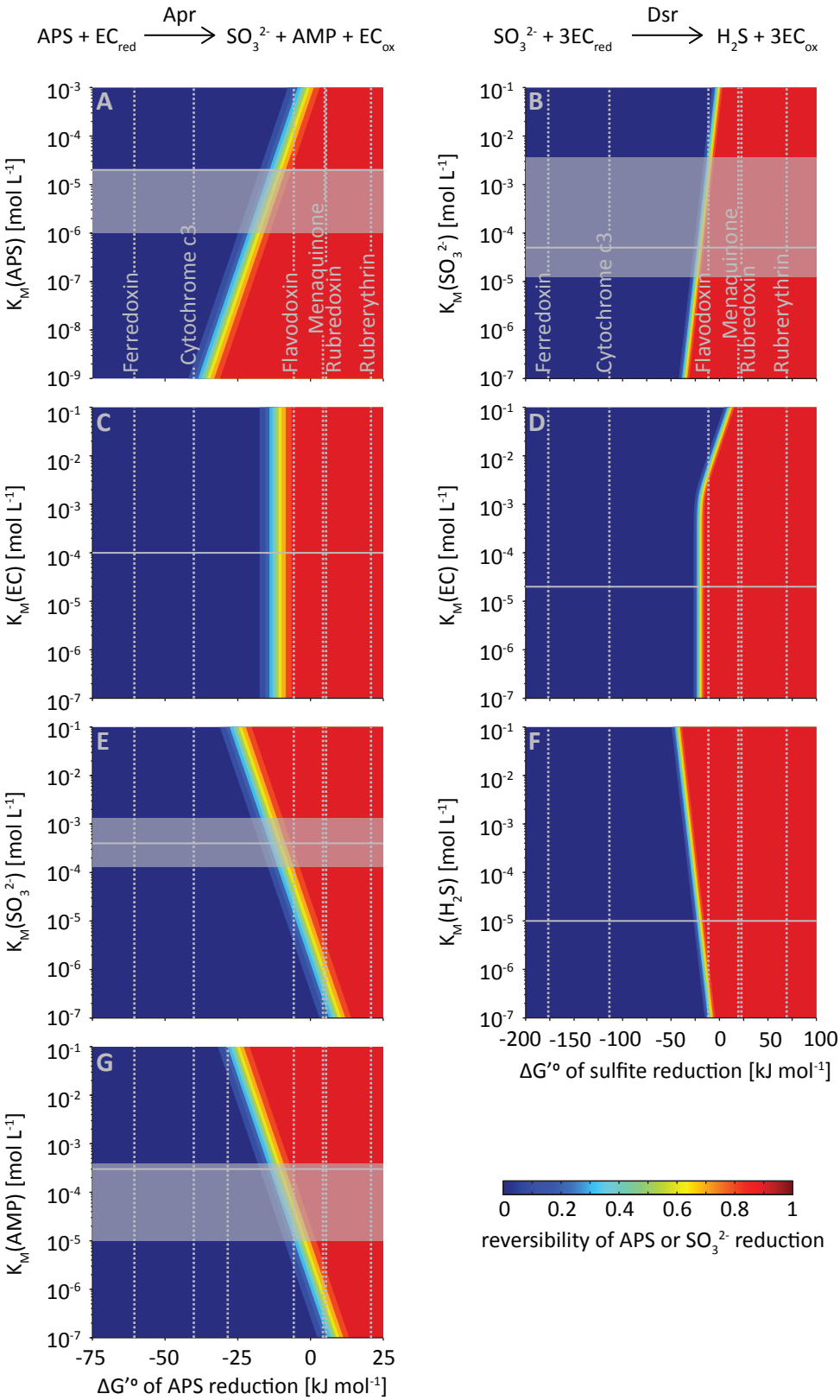

Figure S1. Reversibility of APS (left), and sulfite reduction (right) as a function of enzyme half-saturation constants (K_M) and Gibbs free energies of reactions at standard conditions (ΔG'°). Full reversibility of APS and SO_3^{2-} reduction, and therefore large fractionation, is only possible when electron carriers with slightly negative to positive reduction potential are involved. Reactions that occur far from equilibrium, lead to net S isotope fractionations that are smaller than the thermodynamic limit, and are therefore inconsistent with observations and culture experiments. The figures are for a csSRR of 0.1 fmol H_2S $cell^{-1}$ day^{-1} and a reduced to oxidized electron carrier ratio ($R_{r/o}$) of 0.01, i.e., on the plateau (see Fig. 4). The horizontal grey lines indicate the parameter values used in the default model, based on the range of available experimental data (shaded boxes; see also Dataset S1). The vertical dashed lines indicate the calculated ΔG'° of the reaction with the respective electron carrier. Ferredoxin is the strongly negative reduction potential form (E'° Fd ox/red ≈ -398 mV); flavodoxin stands for the modestly negative reduction potential form (E'° F/FH ≈ -115 mV).

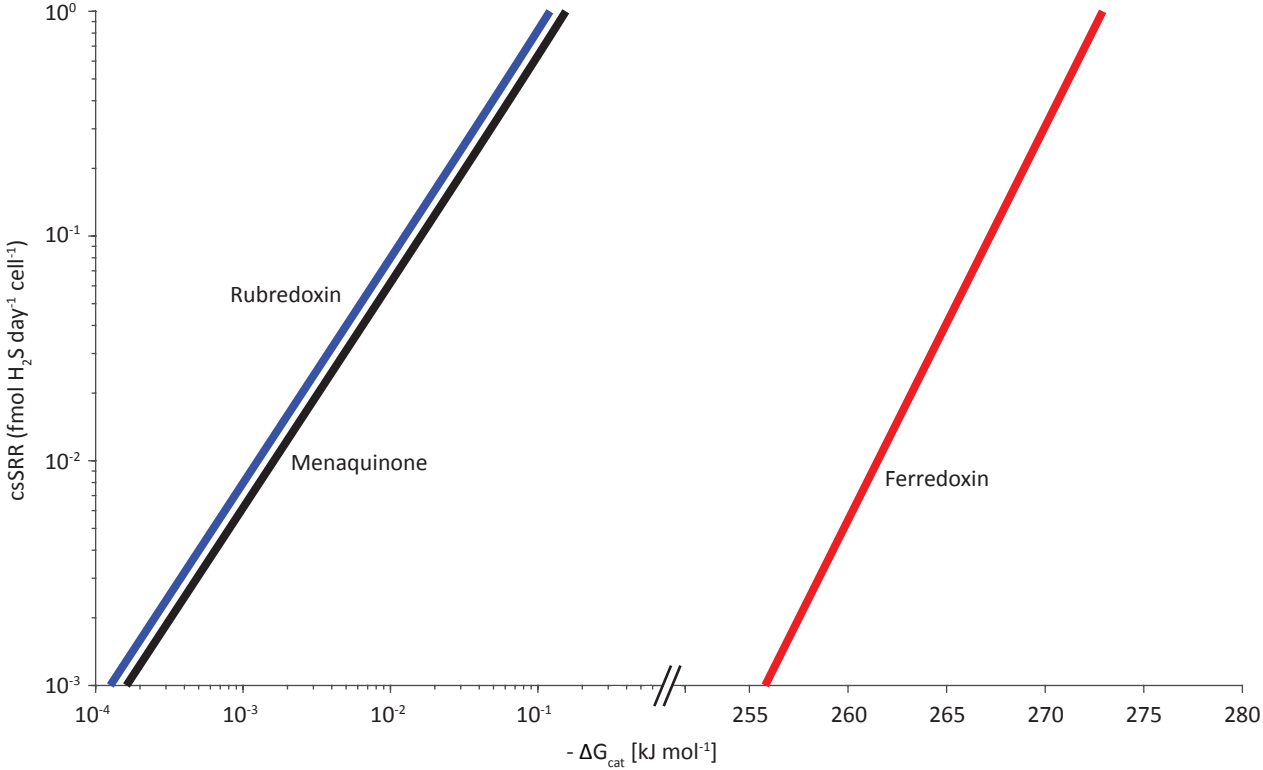

Figure S2. Cell specific sulfate reduction rate as a function of the free energy of the catabolic reation (ΔG_{cat}). The isotope-biochemical model predicts intracellular metabolite concentrations, which determine the Gibbs free energies of each reaction step. The total calcualted free energy is the sum of the free energies of all steps (sulfate uptake, activation to APS, APS reduction, SO_3^{2-} reduction to H_2S) in the theoretical case that APS and sulfite reduction would be coupled to rubredoxin (blue line), menaquinone (black line), or ferredoxin (red line) oxidation. Our results imply that in energy-limited subsurface environments, higher respiration rates are possible when using electron carriers with modestly negative reduction potential such as rubredoxin or menaquinone.